NUCLEAR DATA AND MEASUREMENTS SERIES

ANL/NDM-131

Fast-Neutron Scattering From Vibrational Palladium Nuclei

by

A.B. Smith and P.T. Guenther

October 1993

**ARGONNE NATIONAL LABORATORY,
ARGONNE, ILLINOIS 60439, U.S.A.**

NUCLEAR DATA AND MEASUREMENTS SERIES

ANL/NDM-131

FAST-NEUTRON SCATTERING FROM VIBRATIONAL PALLADIUM NUCLEI

A. B. Smith and P. T. Guenther

October, 1993

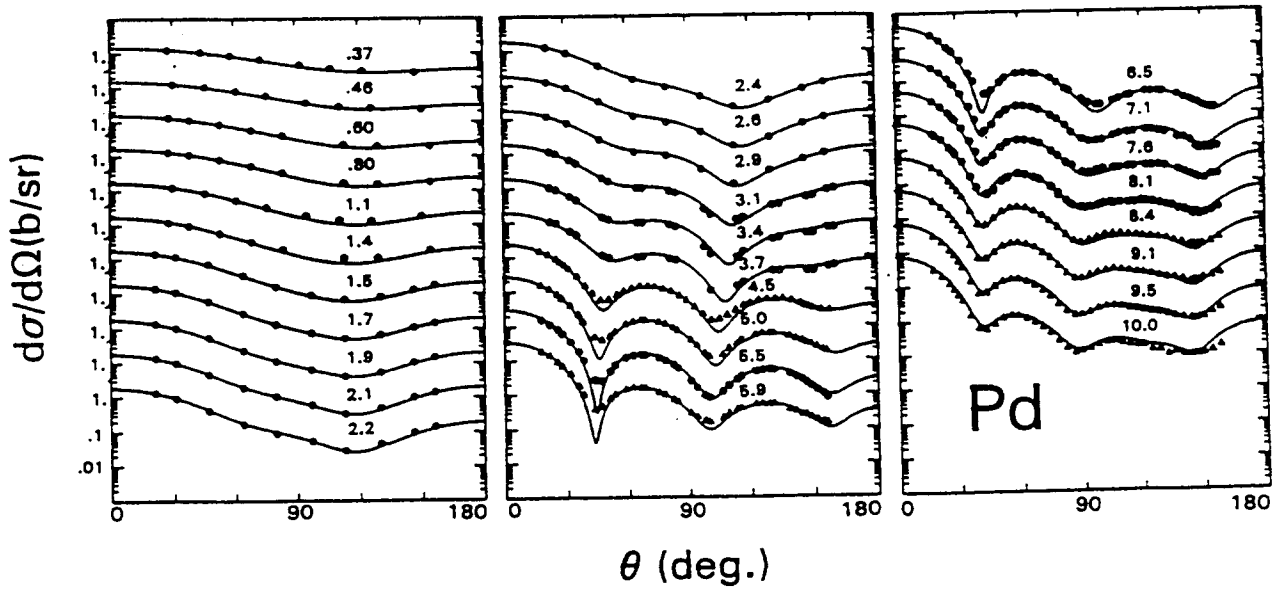

ARGONNE NATIONAL LABORATORY, ARGONNE, ILLINOIS

Operated by THE UNIVERSITY OF CHICAGO

for the U. S. DEPARTMENT OF ENERGY

under Contract W-31-109-Eng-38

Reproduced from the best available copy.

Available to DOE and DOE contractors from the
Office of Scientific and Technical Information
P.O. Box 62
Oak Ridge, TN 37831
Prices available from (615) 576-8401

Available to the public from the
National Technical Information Service
U.S. Department of Commerce
5285 Port Royal Road
Springfield, VA 22161

ANL/NDM-131

FAST-NEUTRON SCATTERING FROM VIBRATIONAL PALLADIUM NUCLEI*

by

A. B. Smith[a,b] and P. T. Guenther[a]

[a]Argonne National Laboratory
Argonne, Illinois

[b]Universtiy of Arizona
Tucson, Arizona

Keywords:

Measured σ_t, $d\sigma/d\Omega_{el}$ and $d\sigma/d\Omega_{inel}$ for $\leq$ 10.0 MeV neutrons incident on elemental palladium. Optical-statistical and coupled-channels models.

Engineering Physics Division
Argonne National Laboratory
9700 South Cass Avenue
Argonne, Illinois 60439
U. S. A

* This work supported by the United States Department of Energy under Contract W-31-109-Eng-38; also under the auspices of The Department of Nuclear and Energy Engineering, College of Engineering and Mines, University of Arizona.

PRIOR ISSUES IN THE ANL/NDM SERIES

A listing of recent issues in this series is given below. Issues and/or titles prior to ANL/NDM-114 can be obtained from the National Technical Information Service, U. S. Department of Commerce, 5285 Port Royal Road, Springfield, VA 22161, or by contacting one of the authors of this report at the following address:-

Engineering Physics Division
Argonne National Laboratory
9700 South Cass Avenue
Argonne, IL 60439
USA

A.B. SMITH, R.D. LAWSON, AND P.T. GUENTHER
Ambiguities in the Elastic Scattering of 8 MeV neutrons from Adjacent Nuclei
ANL/NDM-114, January 1990

A.B. SMITH, S. CHIBA, D.L. SMITH, J.W. MEADOWS, P.T. GUENTHER, R.D. LAWSON, AND R.J. HOWERTON
Evaluated Neutronic File for Indium
ANL/NDM-115, January 1990

S. CHIBA, P.T. GUENTHER, R.D. LAWSON, AND A.B. SMITH
Neutron Scattering from Elemental Indium, the Optical Model, and the Bound-State Potential
ANL/NDM-116, June 1990

D.L. SMITH AND L.P. GERALDO
An Evaluation of the Nb-93(n,n')Nb-93m Dosimeter Reaction for ENDF/B-VI
ANL/NDM-117 (November 1990)

J.W. MEADOWS
Characteristics of the Samples in the FNG Fission Deposit Collection
ANL/NDM-118 (November 1990)

S. CHIBA, P.T. GUENTHER, A.B. SMITH, M. SUGIMOTO, AND R.D. LAWSON
Fast-Neutron Interaction with Elemental Zirconium, and the Dispersive Optical Model
ANL/NDM-119, June 1991

A.B. SMITH, P.T. GUENTHER, J.F. WHALEN, AND S. CHIBA
Fast-neutron Total and Scattering Cross Sections of ^{58}Ni and Nuclear Models
ANL/NDM-120, July 1991

S. CHIBA AND D.L. SMITH
A Suggested Procedure for Resolving an Anomaly in Least-squares Data Analysis Known as "Peelle's Pertinent Puzzle" and the General Implications for Nuclear Data Evaluation
ANL/NDM-121, September 1991

D.L. SMITH AND DOMINIQUE FEAUTRIER
Development and Testing of a Deuterium Gas Target Assembly for Neutron Production Via the H-2(D,N)HE-3 Reaction at a Low-energy Accelerator Facility
ANL/NDM-122, March 1992

D.L. SMITH AND E.T. CHENG
A Review of Nuclear Data Needs and Their Status for Fusion Reactor Technology with some Suggestions on a Strategy to Satisfy the Requirements
ANL/NDM-123, September 1991

J.W. MEADOWS
The Thick-Target $^{9}Be(d,n)$ Neutron Spectra for Deuteron Energies Between 2.6 and 7.0-MeV
ANL/NDM-124, November 1991

A.B. SMITH AND P.T. GUENTHER
Fast-Neutron Scattering Near Shell Closures:- Scandium
ANL/NDM-125, August 1992

A.B. SMITH, J.W. MEADOWS AND R.J. HOWERTON
A Basic Evaluated Neutronic Data File for Elemental Scandium
ANL/NDM-126, September 1992

A.B. SMITH AND P.T. GUENTHER
Fast-Neutron Interaction With Vibrational Cadmium Nuclei
ANL/NDM-127, September 1992

D.L. SMITH
A Least-Squares Computational "Tool kit"
ANL/NDM-128, April 1993

JOSEPH McCABE, A.B. SMITH AND J.W. MEADOWS
Evaluated Nuclear Data Files for the Naturally-Occuring Isotopes ofCadmium
ANL/NDM-129, June 1993

A.B. SMITH AND P.T. GUENTHER
Fast-Neutron Interaction with the Fission Product ^{103}Rh
ANL/NDM-130, September 1993

ANL/NDM-131

FAST-NEUTRON SCATTERING FROM VIBRATIONAL PALLADIUM NUCLEI

by

A. B. Smith and P. T. Guenther

ABSTRACT

Neutron total cross sections of elemental palladium are measured from ≈ 0.6 → 4.5 MeV. These results, combined with others previously reported from this laboratory, provide a detailed knowledge of the neutron total cross sections of palladium from ≈ 0.1 → 20 MeV. Differential neutron elastic-scattering cross sections are measured from ≈ 1.5 → 10 MeV in sufficient energy and angle detail to well define the energy-average behavior. Concurrently, neutron inelastic-scattering cross sections are measured from ≈ 1.5 → 8 MeV. Inelastically-scattered neutron groups are observed corresponding to excitations of; 306 ± 14, 411 ± 47, ≈ 494, 791 ± 20, 924 ± 20, 1156 ± 24, 1358 ± 35, 1554 ± 47 and 1706 ± 59 keV, with additional tentative groups at 1938 and 2059 keV. Particular attention is given to the inelastic excitation of the 2^+ yrast states of the even isotopes. This broad data base is examined in the context of optical-statistical and coupled-channels models. The resulting model parameters are consistent with systematic trends in this vibrational mass region previously noted at this laboratory, and provide a suitable vehicle for many applications.

TABLE OF CONTENTS

I. INTRODUCTION

Elemental palladium consists of the six isotopes ^{102}Pd (1.02%), ^{104}Pd (11.14%), ^{105}Pd (22.33%), ^{106}Pd (27.33%), ^{108}Pd (26.46%) and ^{110}Pd(11.72%). These, and the unstable isotopes of palladium, are prominent fission products and are known to be very strong collective vibrators [1]. More than three quarters of the element consists of even isotopes whose prominent feature is a one-phonon level at $\approx$ 350 → 550 keV and the two-phonon triad of levels at $\approx$ 800 → 1350 keV [1]. The inelastic-neutron-scattering cross sections for the excitation of the one-phonon level is known to be large [2], and therefore of importance in the context of a number of applications (for example, in FBR fuel-cycle and incineration considerations). There has been considerable interest in the direct neutron inelastic-scattering processes associated with the excitation of the one-phonon states of the even isotopes [3], and in the macroscopic quadrupole collective model for states excited by heavy-ion coulomb-excitation processes [4].

Because of the applied and fundamental importance, the neutron interaction with palladium has been studied by this Group for a quarter of a century. Neutron total and scattering cross sections at energies of $\leq$ 1.5 MeV were reported in ref. [5]. A preliminary report of the present work over the energy range $\approx$ 1.5 → 4.0 MeV was given in ref. [2], and some of that material was used in the survey study of ref. [6]. The results of several isolated measurements at $\approx$ 7.5 MeV were reported in ref. [7]. These endeavors have now been enlarged to a detailed study of the neutron interaction with palladium from 1.5 → 10 MeV. This paper reports these comprehensive measured values and their model interpretations, extended to lower energies with the earlier work of ref. [5]. The objective was to provide quantitative information for application purposes and to enhance the fundamental understanding of the the fast-neutron interaction in this region of strong collective vibrations.

Subsequent portions of this paper deal with; II) experimental methods, III) experimental results, and IV) physical models. Some aspects of the results are discussed and summarized in Section V).

II. EXPERIMENTAL METHODS

The experimental methods employed in this work were similar to those used at this laboratory for a number of years. In particular, the measurements were made approximately concurrently with recent ^{58}Ni [8], zirconium [9], cadmium [10] and ^{103}Rh [11] studies. Details of

the measurement techniques can be found in these references, and citations given therein. Therefore, only an outline of the experimental methods is given here.

The sample used in all the measurements was a metallic cylinder of elemental palladium, 2 cm in diameter and 2 cm long. It was believed to be free of voids, and it had a chemical purity of >99%. Sample densities were determined by conventional weight and dimensional measurements to at least 0.1% accuracies. In the total-cross-section transmission measurements, neutrons were incident upon the base of the cylinder. In the scattering measurements they were incident on the lateral surface.

The total cross section measurements were made using a cyclic monoenergetic technique. The method is described in ref. [2], and is similar to the method used in the white-source measurements of ref. [12]. Those interested in the experimental details should refer to these references.

The neutron scattering measurements were made using the fast-neutron time-of-flight technique [13,14]. The $^{7}Li(p,n)^{7}Be$ reaction was used as a neutron source at neutron energies of ≤ 4 MeV [15]. The lithium target was a metal film, adjusted for the desired neutron-energy spread. Above 4 MeV, the $D(d,n)^{3}He$ reaction was employed as the source [15]. The deuterium was contained in a gas cell with a pressure selected for the desired incident-neutron energy resolutions. In both cases, the mean neutron energy was determined to ≤ 20 keV by magnetic analysis of the incident ion beam. Both sources were pulsed at a repetition rate of 2 MHz, with burst durations of ≈ 1 nsec. Burst intensity was enhanced by the use of a harmonic bunching system. The scattering sample was placed ≈ 18 cm from the source at a 0° source-reaction angle, and at the focus of ten heavily-shielded scattered-neutron collimators. These collimators were distributed over an angular range of $\approx 17^{\circ} \rightarrow 160^{\circ}$. An additional time-of-flight channel was arranged to view the source alone, and was used for monitoring the source intensity. The relative angular scale of the collimated flight paths was optically defined to $< 0.1^{\circ}$, and the 0° normalization of the angular scale was determined to $\approx 0.1^{\circ}$ by the observation of neutrons scattered both left and right of the apparent center line. There was an additional estimated angular uncertainty of $< 0.3^{\circ}$ due to very small shifts of the shape and/or position of the ion beam as it struck the targets. Most of the scattering measurements were made with flight paths of ≈ 500 cm. A few higher-resolution measurements were made with flight paths of $15 \rightarrow 18$ m. One of these was fixed at 80° and very heavily shielded. The others were variable over the above angular range and less-heavily shielded. The resulting scattered-neutron resolutions were ≈ 0.6

nsec/m (at 5 m), and ≤ 0.2 nsec/m (at the longer flight paths). All the neutron detectors were hydrogenous scintillators. Those used at ≈ 5 m were 12.5 cm in diameter with thicknesses of ≈ 2 cm (at energies below 4 MeV) and of ≈ 6 cm (at higher energies). The detectors used at the longer flight paths were ≈ 25 cm in diameter and ≈ 5 cm thick. γ-ray backgrounds in all the detectors were suppressed by using pulse-shape-selection techniques. The relative energy dependencies of the detectors were determined by the observation of neutrons emitted at the spontaneous fission of ^{252}Cf in the manner described in ref. [16]. Below 4 MeV, these relative responses were normalized to the total cross sections of carbon, as described in ref. [17]. Above 4 MeV, the normalization was to the well known H(n,n) scattering cross sections [18]. The data acquisition and reduction was carried out using an integrated computer software system [19]. The resulting cross sections were corrected for multiple-event, beam-attenuation and angular-resolution effects using Monte-Carlo techniques as described in ref. [20]. The Monte-Carlo calculations also made a correction for the second neutron group from the $^{7}Li(p,n)^{7}Be$ source reaction where applicable.

III. EXPERIMENTAL RESULTS

A. Neutron Total Cross Sections

Neutron total cross sections were measured from ≈ 0.60 → 4.5 MeV with energy spreads of ≈ 50 keV and at intervals of ≈< 50 keV. Several redundant passes were made over the energy range and the combined results binned into ≈ 50 keV intervals. The statistical uncertainties of the binned values were ≈< 1%. These results were presented in the preliminary report of ref. [2]. Earlier values from this laboratory extend the present results downward to several-hundred keV [5], and more recently white-source results, also obtained at this laboratory, extend the measurements upward to ≈ 20 MeV [12]. The combination of the three sets of values provides a good knowledge of the neutron total cross sections of elemental palladium extending from ≈ 0.1 → 20 MeV. These results are also consistent with major sets of total-cross-section information available in the literature (e.g., with those of Foster and Glasgow [21]). The present measured total cross sections are compared with those available in the literature, and from refs. [5] and [12], in Fig. III-1. The agreement is excellent.

B. Neutron Elastic-scattering Cross Sections

From ≈ 1.5 → 3 MeV the differential elastic-scattering cross sections were measured with incident-energy intervals and resolutions

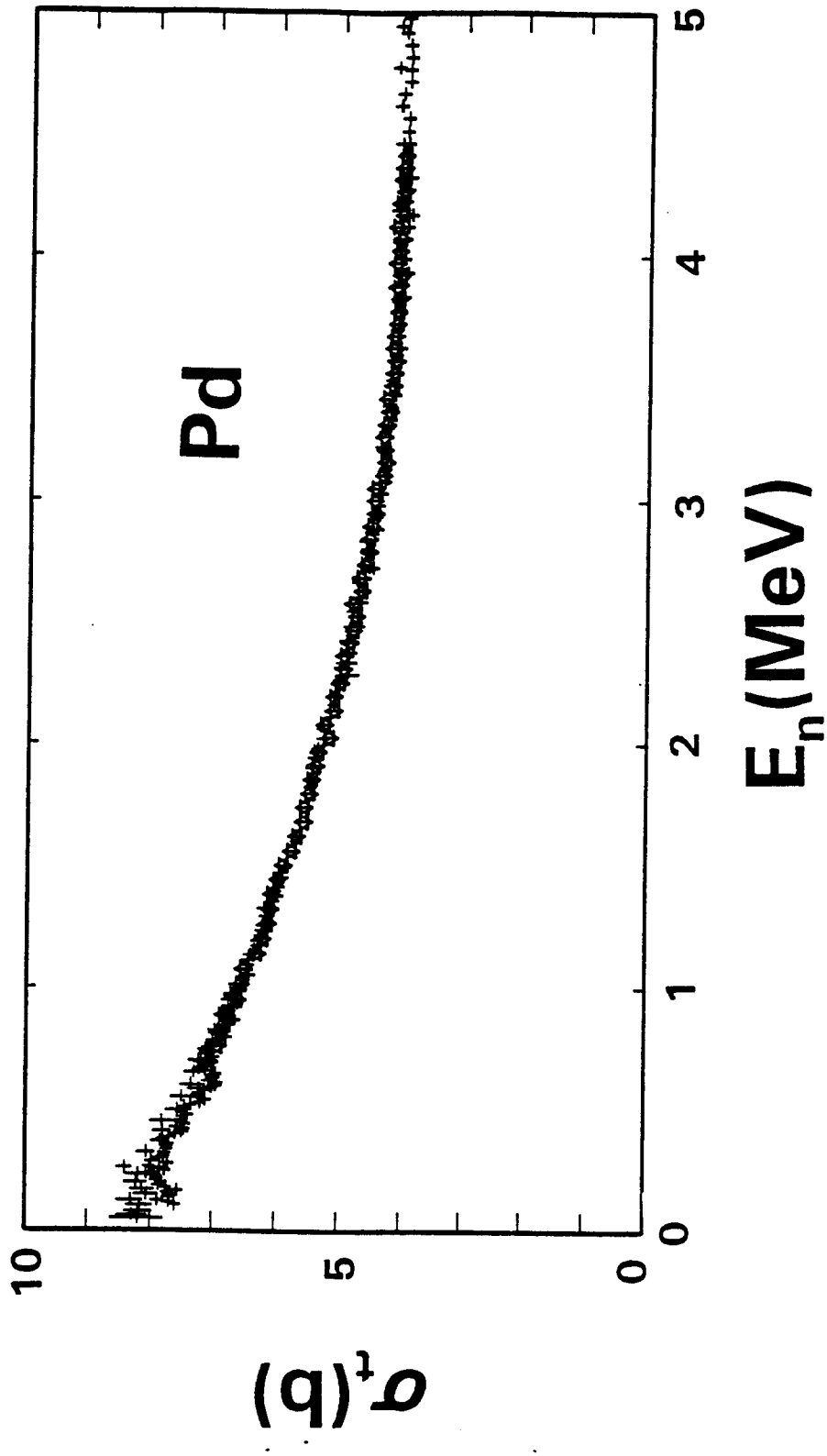

Fig. III-1. Comparisons of measured palladium neutron total cross sections. The present results are indicated by "star" symbols, and those from previous work at this laboratory and from the literature by crosses.

of ≈ 50 keV so as to assure full energy coverage. Ten scattering angles were used, distributed from ≈ 20^{o} → 160^{o}. From ≈ 3 → 4 MeV the measurements were made at ≈ 100 keV incident-energy intervals with ≈ 50 keV energy resolutions, but at ≈ 20 scattering angles distributed over the same angular range. The scattered-neutron resolutions were sufficient to determine the elastic-scattering contribution free from inelastic-scattering perturbations. A running 200 keV average of the measured values was constructed in order to smooth any possible physical or experimental fluctuations, with the results shown in Fig. III-2. Statistical uncertainties of the differential values ranged from < 1% to larger values at the minima of the distributions. Systematic uncertainties were estimated to be ≈ 3.5%, with a small additional factor, due to the angular uncertainty, that varied depending upon the anisotropy of the distributions. These results extrapolate reasonably well to the lower-energy values of ref. [5].

Above 4 MeV the differential elastic-scattering cross sections were determined at ≈ 500 keV incident-energy intervals and at forty or more scattering angles distributed between ≈ 17^{o} and 160^{o}. Incident-neutron energy spreads decreased with energy from ≈ 350 keV at 4.5 MeV to ≈ 100 keV at 10 MeV. The scattered-neutron resolution obtained with the 5 m flight path was sufficient to resolve the elastic-scattering component from that due to the excitation of the first level in the even isotopes over the incident-energy range of ≈ 5.5 → 8.0 MeV. In this range the data was processed to obtain "elastic" scattering distributions both inclusive and exclusive of inelastic contributions due to the excitations of levels at ≤ 0.6 MeV. From 4.5 → 5.5 MeV the scattered-neutron resolution deteriorated due to the increasing thickness of the deuterium gas target. At these lower energies the measured "elastic" scattering cross sections were obtained by processing the velocity spectra so as to include inelastically-scattered neutrons corresponding to excitations of ≤ 0.6 MeV. Above incident energies of ≈ 8 MeV the scattered-neutron resolution was insufficient to resolve the inelastically-scattered neutrons due to the excitation of levels at ≤ 0.6 MeV. Thus, again, the measured velocity distributions were analyzed so as to include all inelastic contributions up to excitations of ≤ 0.6 MeV. Above 4 MeV none of the elastic scattering measurements resolved the neutrons due to the excitation of the first four to five levels of the odd isotope ^{105}Pd from the elastically-scattered component. As shown later, the the compound-nucleus portion of these cross sections is not large and the isotope is only 22% abundant. These inelastic-scattering perturbations of the elastic distributions were considered in the interpretations described below.

At incident energies of ≈ 5.9 → 8.0 MeV the apparent resolution of the elastic scattering obtained from the 5 m flight-path measurements was verified by a few angular-distribution measurements

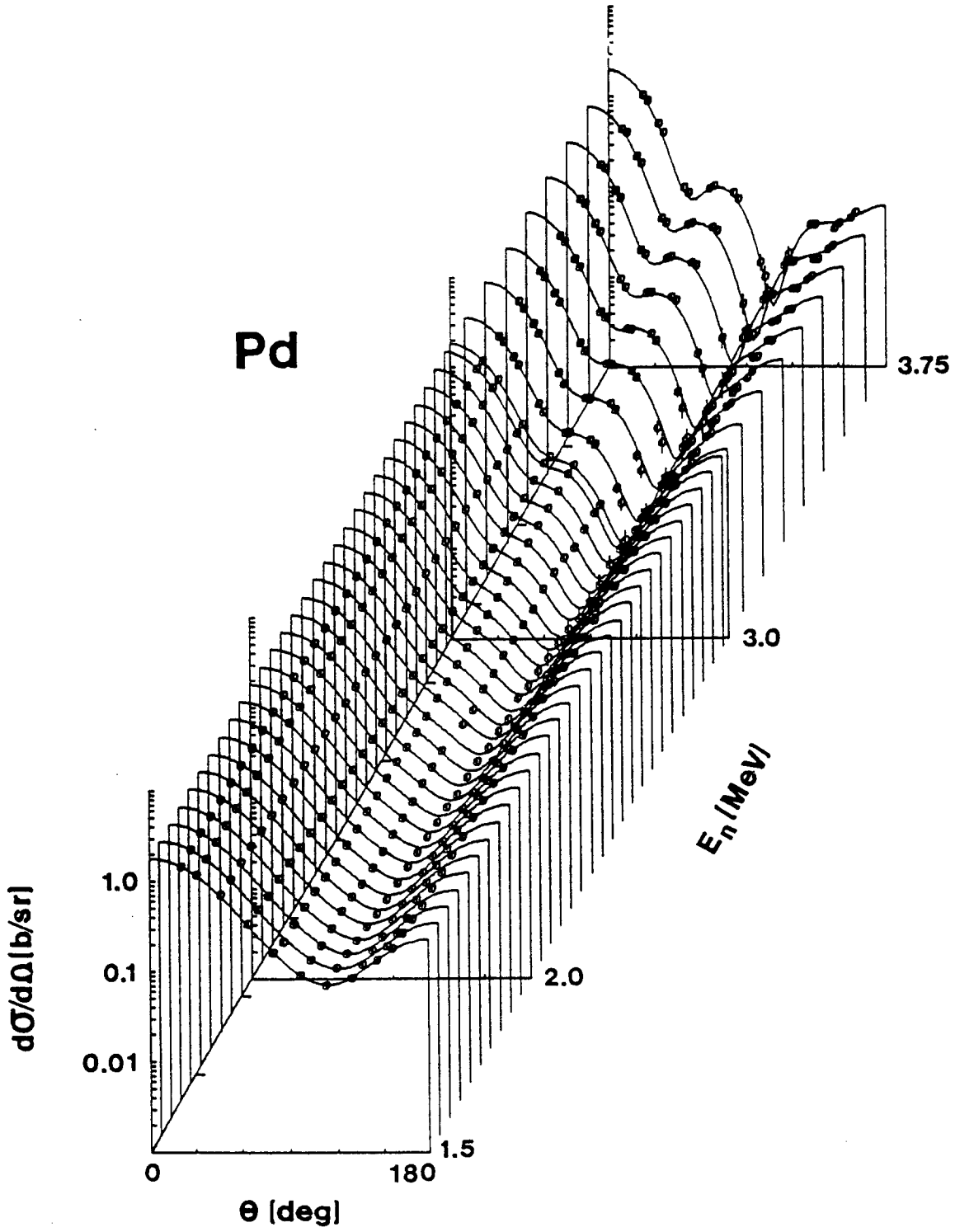

Fig. III-2. Differential elastic-scattering cross sections of palladium in the incident energy range ≈ 1.5 → 4 MeV. The present measurements are indicated by symbols, and curves show the results of fitting Legendre-polynomial expansions to the experimental values. Throughout this work the angle-differential data are given in the laboratory coordinate system.

made at flight paths of ≈ 15 → 18 m. The scattering angles were limited to five but the resolutions were very good and clearly separated elastically and inelastically-scattered contributions from the even isotopes, as illustrated in Fig. III-3. The same approach was not suitable in the 4.5 → 5.5 MeV range as the deuterium target thickness required for reasonable intensity remains an obstacle, and the rapid increase with energy of the second neutron-group intensity from the lithium target makes its use impractical.

The statistical accuracies of the measured differential elastic-scattering cross sections above 4 MeV ranged from < 1% at forward angles to larger values in the minima of the distributions. In addition there were systematic uncertainties of 2 → 3%, including contributions from detector normalization, angular uncertainties and the correction procedures.

With the above caveats, the elastic-scattering results above 4 MeV are shown in Fig. III-4. The same figure shows an ≈ 250 keV average of the 1.5 → 4 MeV results of Fig. III-2, and below 1.5 MeV a similar ≈ 200 keV average of the results of ref. [5]. The literature contains essentially no prior experimental information comparable with the present results, other than that previously obtained at this laboratory.

C. Neutron Inelastic-scattering Cross Sections

The six isotopes of palladium collectively have over one hundred levels with excitations of less than 2 MeV. Those with reasonably-established J^{π} values are listed in Table III-1, which ignores the low-abundance ^{102}Pd. With this profusion of levels it was not possible to resolve the inelastic-neutron excitation of any isolated level. Rather, the observed inelastically-scattered neutron groups were composite excitations due to contributions from several or clumps of levels. This complexity is schematically illustrated in Fig. III-5 where the excitation energies (indicated by bars) are compared with the observed neutron groups (stars). The magnitudes of the bars corresponds to the respective isotopic abundances, and, of course, cross sections will be further modulated by J^{π} values and channel competition.

Inelastically-scattered neutron groups corresponding to composite excitations of 306 ± 14, 411 ± 47, ≈ 494, 791 ± 20, 924 20, 1156 ± 24, 1358 ± 35, 1554 ± 47, and 1706 ± 59 keV were observed. The cited uncertainties are RMS deviations of a number of measurements

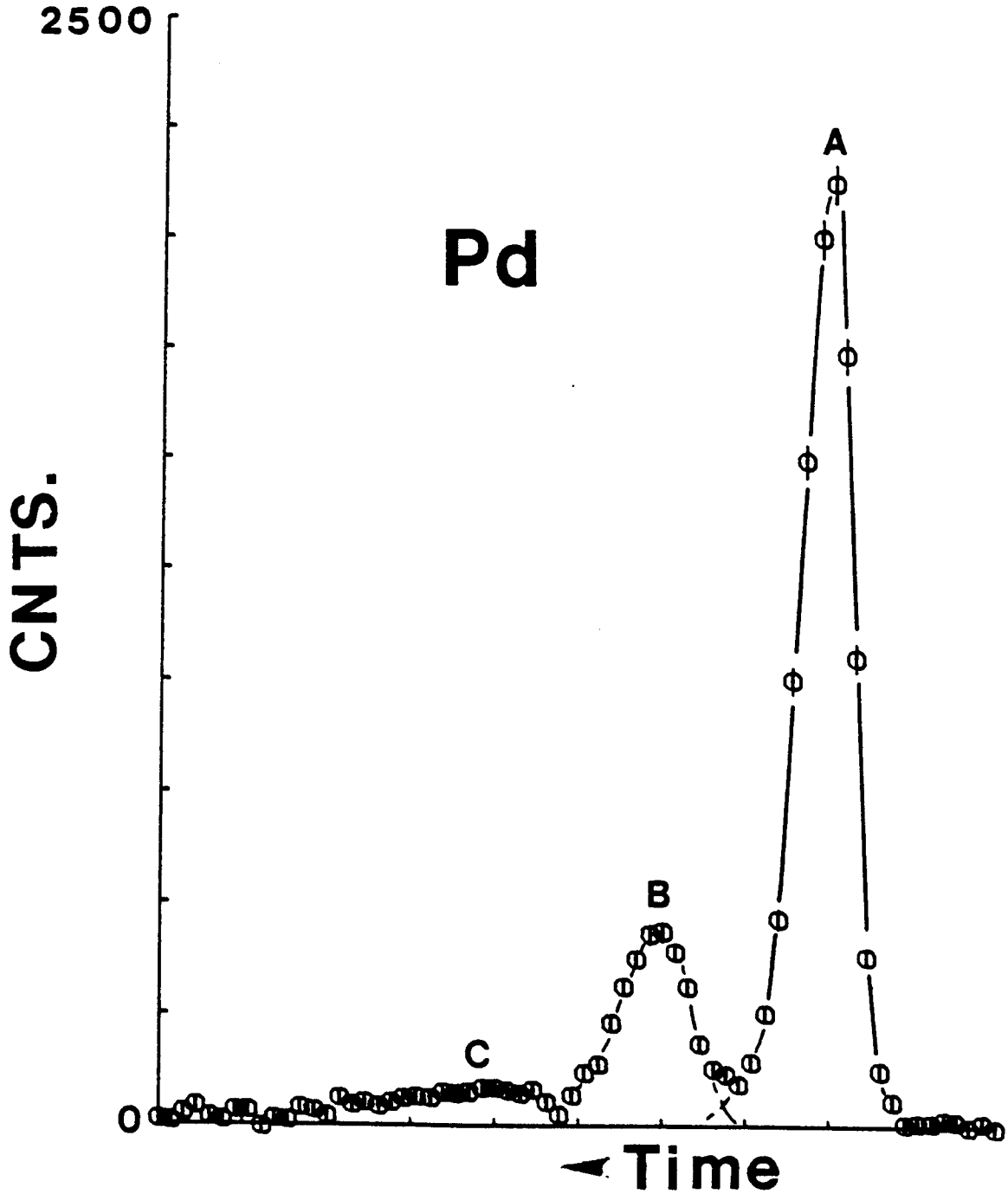

Fig. III-3. Illustrative scattered-neutron time distribution. The incident energy was 7.14 MeV, the flight path 15.8 m and the scattering angle 80^{o}. The "A" peak is due to elastic scattering, "B" is primarily due to inelastic scattering from the first 2^{+} levels of the even isotopes, and the "C" continuum results from a number of inelastic-scattering contributions from the odd isotope ^{105}Pd.

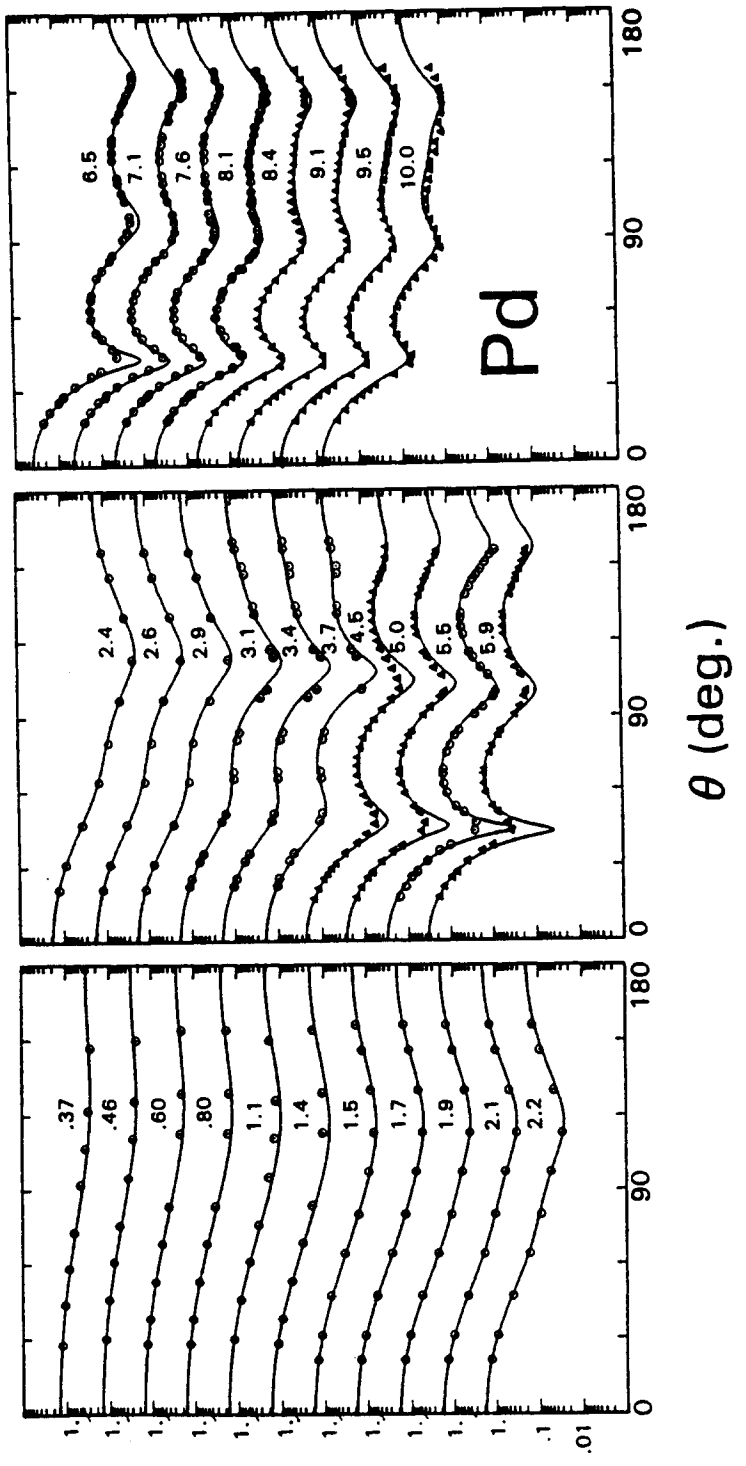

Fig. III-4. Measured and calculated elastic-scattering cross sections of palladium. Experimental results are indicated by symbols where "O" is elastic scattering and "Δ" elastic scattering inclusive of inelastic contributions for excitations of ≤ 600 keV. Curves denote the results of SOM calculations. 250 keV averages of present results are shown between 1.5 → 4 MeV, and 200 keV averages of the data of ref. [5] below 1.5 MeV, as described in Section IV-A of the text.

Table III-1. Low-lying excitations of the five isotopes of elemental Palladium. Excitation energies (in MeV) and J^{π} values are taken from ref. [1].

Isotope 104		105		106		108		110	
E_x	(J^{π})	E_x	(J^{π})	E_x	(J^{π})	E_x	(J^{π})	E_x	(J^{π})
0.000	(0^+)	0.000	$(5/2^+)$	0.000	(0^+)	0.000	(0^+)	0.000	(0^+)
0.556	(2^+)	0.281	$(3/2^+)$	0.512	(2^+)	0.434	(2^+)	0.374	(2^+)
1.324	(4^+)	0.306	$(7/2^+)$	1.128	(2^+)	0.931	(2^+)	0.814	(2^+)
1.334	(0^+)	0.319	$(5/2^+)$	1.134	(0^+)	1.048	(4^+)	0.921	(4^+)
1.342	(2^+)	0.345	$(1/2^+)$	1.229	(4^+)	1.053	(0^+)	0.947	(0^+)
1.793	(0^+)	0.442	$(7/2^+)^*$	1.558	(3^+)	1.314	(0^+)	1.171	(0^+)
1.794	(2^+)	0.447	$(3/2^+)^*$	1.562	(2^+)	1.335	$(4^+)^*$	1.212	$(3^+)^*$
1.821	(3^+)	0.489	$(11/2^-)$	1.706	(0^+)	1.441	(2^+)	1.214	$(2^+)^*$
1.999	$(1^+)^*$	0.561	$(5/2^+)$	1.909	(1^+)	1.540	$(2^+)^*$	1.398	$(2^+)^*$
2.082	(4^+)	0.645	$(7/2^-)$	1.932	(4^+)	1.625	$(4^+)^*$	1.470	$(2^+)^*$
		0.651	$(3/2^+)$	2.001	(0^+)	1.771	(6^+)	1.574	$(6^+)^*$
		0.673	$(1/2^+)^*$			1.956	(4^+)	1.719	$(4^+)^*$
		0.697	$(7/2^+)^*$			1.989	$(4^+)^*$	1.890	$(2^+)^*$
		0.727	$(5/2^+)$						
		0.782	$(9/2^+)$						

* Tentative assignments. These values were used in the interpretations of Section IV.

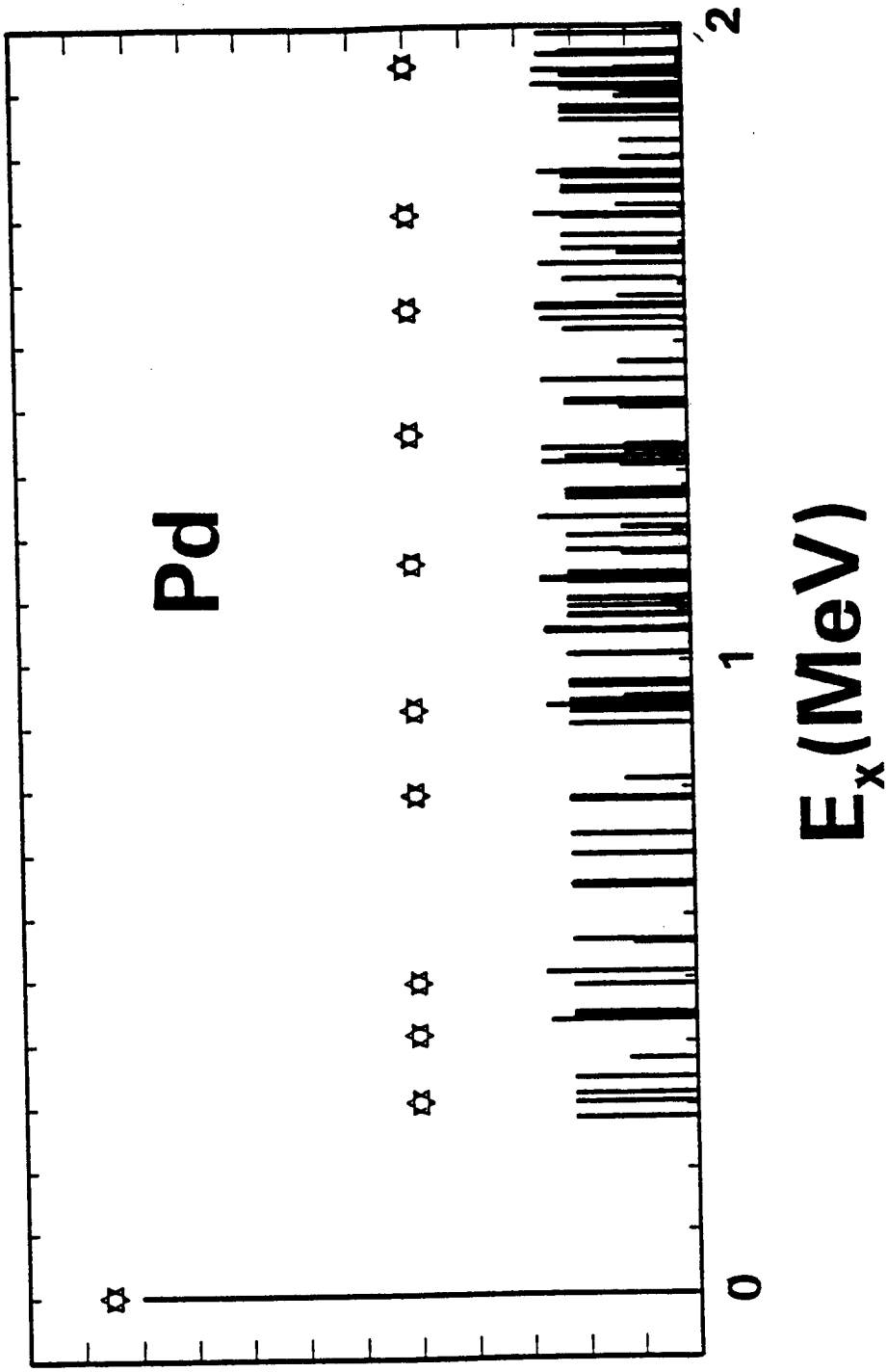

Fig. III-5. Schematic comparison of reported [1] (bars) and observed (stars) inelastic neutron excitations in elemental palladium. The figure is further defined in the text.

from the means and not scattered-neutron resolutions. In addition, groups of neutrons were tentatively observed corresponding to excitations of 1938 and 2059 keV. The observed 306 keV level appears to be due entirely to levels in the odd isotope ^{105}Pd. The 411 keV level is probably due to contributions from ^{105,108} and ^{110}Pd, and the 494 keV level to ^{102,104,105} and ^{106}Pd contributions. The detailed specification of the latter observed excitation is further complicated by the presence of the second neutron group from the $Li^7(p,n)Be^7$ source reaction and thus an uncertainty was not assigned to the excitation energy. The observed 791 keV excitation is at least due to 105 and ^{110}Pd, and the 924 keV excitation to contributions from 105,108 and ^{110}Pd. Higher-energy observed excitations must consist of contributions from many levels in a number of isotopes.

Cross sections for the above cited inelastic excitations were determined by fitting the observed differential distributions with Legendre-polynomial expansions. Below $\approx$ 4 MeV the observed angular distributions were approximately symmetric about 90^0 and approached isotropy, as one might expect from primarily compound-nucleus (CN) processes. Above 4 MeV only the inelastic scattering due to the sum of excitations of $\leq$ 600 keV was measured, with some uncertainties due to contributions from the ^{105}Pd isotope. The corresponding angular distributions became increasingly anisotropic with energy, with the strong forward peaking indicative of direct-reaction (DR) processes, as illustrated in Fig. III-6. At these higher energies the inelastically-scattered neutrons were not well resolved at very forward angles leading to uncertainties in the determination of the angle-integrated cross-section values. The resulting angle-integrated inelastic-scattering cross sections at incident energies of $<$ 4 MeV are shown in Fig. III-7. In this figure, the illustrated 494 keV excitation is the sum of all observed groups up to excitations of $\approx$ 600 keV. This sum includes contributions from all the yrast 2^+ states of the even isotopes plus a portion of the equivalent contributions from the odd isotope. It was the sum of components that was measured over most of the experimental energy range. Apparently, prior knowledge of inelastic-neutron scattering from palladium is largely confined to the lower-energy ($\leq$ 1.5 MeV) results of ref. [5] which reasonably extrapolate to the present values, as shown in Fig. III-7.

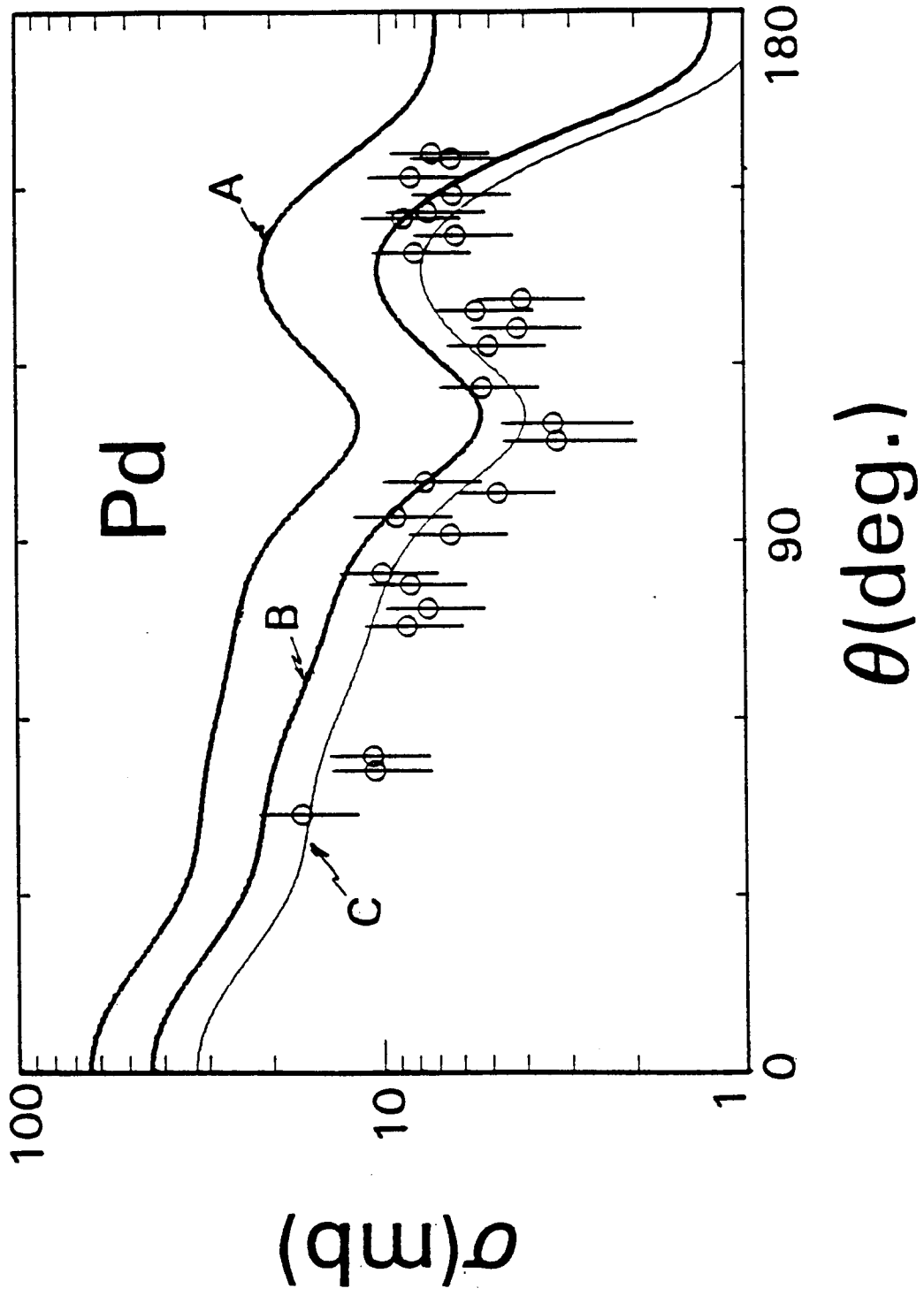

Fig. III-6. Comparison of measured (symbols) and calculated (curves) inelastic-scattering cross sections of palladium due to excitations of $\leq$ 600 keV, as described in the text. The incident energy in this example is 6.5 MeV. Curve "A" was obtained with the one-phonon model, curve "B" with the one- and two-phonon model, and the light curve "C" is "B" X 0.75.

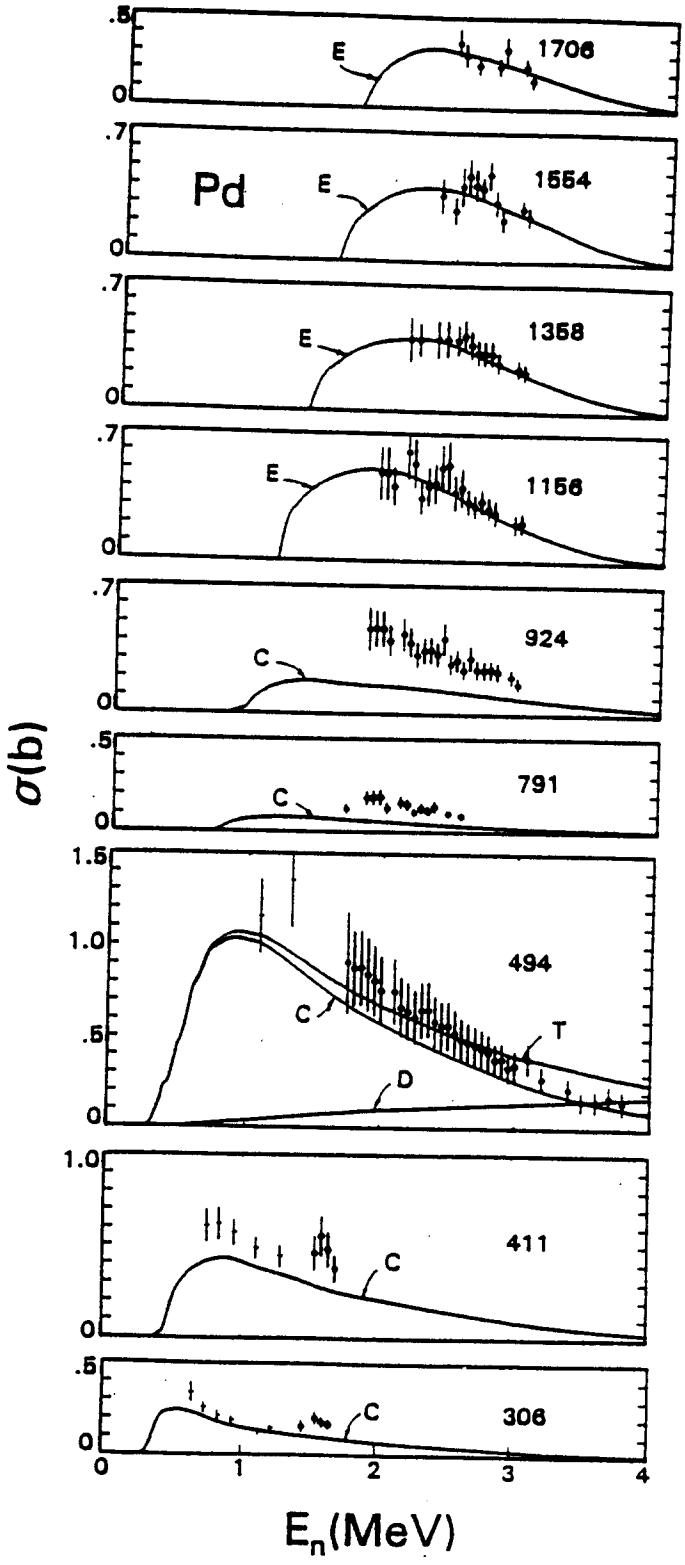

Fig. III-7. Comparisons of measured and calculated inelastic-neutron excitation cross sections of palladium. The present experimental results are indicated by "0" symbols and those of ref. [5] by "+" symbols. Excitation energies are numerically given in keV. Curves are as follows:- "C" calculated CN contributions, "D" calculated DR contributions, "T" the sum C + D, and "E" eyeguides. The 494 keV excitation is the sum of contributions from excitations of < 600 keV, as discussed in the text.

IV. PHYSICAL INTERPRETATION

The objective of the interpretations was the provision of models suitable for basic and applied purposes and the assessment of model properties and systematics in this mass-energy region. The interpretations were based primarily upon the elastic-scattering data, with secondary consideration of total cross sections, inelastic-scattering processes, and strength functions.

A The Data Base

The primary data base for the model derivations is the measured elastic scattering of this work, extended to lower energies using the previous results obtained at this laboratory as given in ref. [5]. This is a large data base that is difficult to handle in the extensive calculations. Therefore, the elastic-scattering results of ref. [5] were averaged over ≈ 200 keV and the 1.5 → 4 MeV results of the present work were averaged over ≈ 250 keV. Above 4 MeV the results of the present work were explicitly used. This elastic-scattering data base is illustrated in Fig. III-4. The total cross section data base consisted of the results of the present work, the values of refs. [5] and [12], and a collection of previously reported values as available at the National Nuclear Data Center [22]. These total cross sections were assembled and evaluated as described in ref. [23], and references for the individual works are cited therein. Strength functions were taken from the well-known compilation of ref. [24].

B. The Spherical Optical-Statistical Model (SOM)

The SOM interpretation is complicated by the multi-isotopic nature of the elemental target, leading to a number of compound-nucleus (CN) and direct-reaction (DR) channels. Inherently, the SOM can not account for the latter. The isotope ^{102}Pd is only ≈ 1% abundant. Therefore, throughout these interpretations it was assumed that the element consisted only of the other five isotopes with the abundances correspondingly normalized for a total of 100%. The discrete excited level structure given in Table III-1, taken from ref. [1], was assumed. Where ref. [1] assigns only tentative J^π values, one of the suggestions was assumed. These J^π uncertainties were at relatively-high excitations and as a consequence alternate choices would have negligible effect on the model development. For excitations above the discrete levels of Table III-1, the statistical representation of Gilbert and Cameron [25] was used. CN contributions from each of the levels were calculated using the Hauser-Feshbach formula [26], corrected for resonance width-fluctuation and correlation effects using the method of Moldauer [27]. All of the SOM calculations employed a special version of the computer code ABAREX

[28] which explicitly treats isotopic components of the element in both simple calculations and in fitting procedures. In doing so both size effects (i.e., $R_i = r_i \cdot A^{1/3}$) and isovector strengths were considered, where the real isovector strength was taken to be 24 MeV and that of the imaginary potential 12 MeV [29]. The model calculations were more sensitive to size than isovector effects. In this palladium case, five isotopes are treated and the length of the calculations is increased, relative to that for a single isotope, by a corresponding factor.

The SOM was primarily based upon explicit fitting of the elastic-scattering distributions shown in Fig. III-4. There are uncertainties in this data base due to scattered-neutron resolutions near ≈ 5.0 MeV and above ≈ 8.4 MeV, as noted in Section III. The data was assumed to have the indicated errors, as reported in the particular measurements. The sequence of the fitting was the determination of; i) the real potential geometry, ii) the imaginary potential geometry, and iii) the real and imaginary strengths. This approach has been frequently used at this laboratory, and reflects the tendency for the real potential to be of a global nature, while the imaginary potential may reflect specific structure effects. The sequence was implemented by six-parameter fitting to obtain the real diffuseness (a_v), five-parameter fitting (a_v fixed) to obtain the real radius (r_v), four parameter fitting (a_v and r_v fixed) to give the imaginary radius (r_w), three parameter fitting (a_v, r_v and r_w fixed) to give the imaginary diffuseness (a_w), and finally two parameter fitting to obtain the real and imaginary strengths (J_v and J_w, respectively). Throughout this paper radii are expressed in the reduced form $R_i = r_i \cdot A^{1/3}$ and potential strengths given in terms of volume-integrals-per-nucleon, J, unless otherwise stated. Apparently, there is no experimental neutron-polarization information for palladium. Therefore, the global real spin-orbit potential of Walter and Guss was used [30]. Potential forms were assumed to be; Saxon-Woods (SW) real potential, SW-derivative imaginary potential, and a Thomas spin-orbit potential [31].

Following the above-outlined fitting procedure, the SOM parameters of Table IV-1 were obtained (These parameters are referenced to the elemental mass A = 106.7. They apply to the isotopes when the size and isovector effects are taken into account). The energy dependencies of the real and imaginary potential strengths are shown in Fig. IV-1. These parameters have some characteristic physical aspects that are discussed in Section V. They give a reasonable description of the data base from which they were developed, as shown in Fig. III-4. There are some discrepancies in the 4.5 - 6.0 MeV range, and possibly above ≈ 8.5 MeV, but both areas are less reliable. The calculated total cross section is compared

with measured values in Fig. IV-2, The agreement with the experimental values is good up to ≈ 7 MeV, while at higher energies the calculated results are up to ≈ 6% larger then the measured values. The SOM calculations also provide CN inelastic-scattering cross sections that are consistent with the experimental values up to excitations of ≈ 600 keV, as shown in Fig. III-6. Of course, the SOM can not describe the direct excitation of the yrast 2^+ levels, and there remains uncertainty as to the explicit correlation of the reported level structure and the observed inelastically-scattered neutron groups. Above excitations of ≈ 600 keV, the calculated results fall considerably short of the measured values. This is not surprising as the calculations have probably missed a number of levels, particularly the case of the odd isotope ^{105}Pd (see Table III-1). Above excitations of ≈ 1 MeV, level uncertainties make comparisons of calculated and measured excitation cross sections so unreliable that they were not attempted. Strength functions calculated with the SOM are compared with those deduced from resonance measurements in Table IV-2. The agreement is reasonable given the small values of S_0 in this mass region, and the scatter of the experimental values. The fact that the small S_0 values are reasonably represented is partly due to the relatively large r_w of Table IV-1. A similar approach was used long ago by Moldauer [32].

C. The Coupled-Channels Model (CCM)

In order to make the calculations viable, a simple one-phonon vibrational model was used in the CCM fitting. It was assumed that elemental palladium could be approximated by a single even isotope having the elemental mass of 106.7, a ground-state spin of 0^+ and a single one-phonon 2^+ state at an excitation energy of 470 keV with simple coupling to the ground state. The excitation energy was the weighted average of the yrast 2^+ excitations of the even palladium isotopes, and should be inclusive of the majority of the components of an analogous excitation of the odd isotope. Initially a $\beta_2 = 0.235$ was assumed, again a weighted average of those of the even isotopes of palladium as determined from EM studies [33]. The model considered only direct-reaction processes, and was based upon the observed elastic scattering, following the same sequence of fitting procedures outlined above for the SOM interpretation. The experimental data base (Fig. III-4) was corrected for CN contributions using the SOM before fitting to determine the CCM parameters. These corrections were very large at low energies. Therefore, CCM fitting was attempted only at energies greater than ≈ 1.5 MeV. Some of the data base did not resolve the elastic scattering from the inelastic contribution due to the excitation of states at ≤ 0.6 MeV. This was particularly so at 4.5 and 5.0 MeV and above 8.4 MeV, and above 4 MeV the observed

Table IV-1. Palladium SOM parameters determined from the fitting procedures of the text. Energies, E, are in Mev and potential strengths, J, in volume-integrals-per-nucleon except for the spin-orbit potential where V_{so} is in MeV.*

Real Potential

$J_v = 465.8 - 4.1055 \cdot E$ MeV-fm^3
$r_v = 1.3079$ fm
$a_v = 0.6638$ fm

Imaginary Potential

$J_w = 109.45 - 5.2146 \cdot E$ MeV-fm^3
$r_w = 1.3801 - 0.0095 \cdot E$ fm
$a_w = 0.3835 + 0.0049 \cdot E$ fm

Spin-Orbit Potential

$v_{so} = 6.043 - 0.015 \cdot E$ MeV
$r_{so} = 1.103$ fm
$a_{so} = 0.560$ fm

---

* Parameters given to precisions that will reproduce the calculations.

Table IV-2. Comparison of SOM strength functions with those deduced from resonance measurements [24] (expressed in units of 10^{-4}).

Isotope	S_0		S_1	
	Exp.	Cal.	Exp.	Cal.
104	----	0.860	5.3±0.5	4.254
105	0.6±0.1	0.864	5.8±0.3	4.164
106	0.35±0.04	0.870	5.7±0.3	4.077
108	0.78±0.17	0.891	4.4±0.5	3.895
110	0.40±0.06	0.925	6.0±0.7	3.706

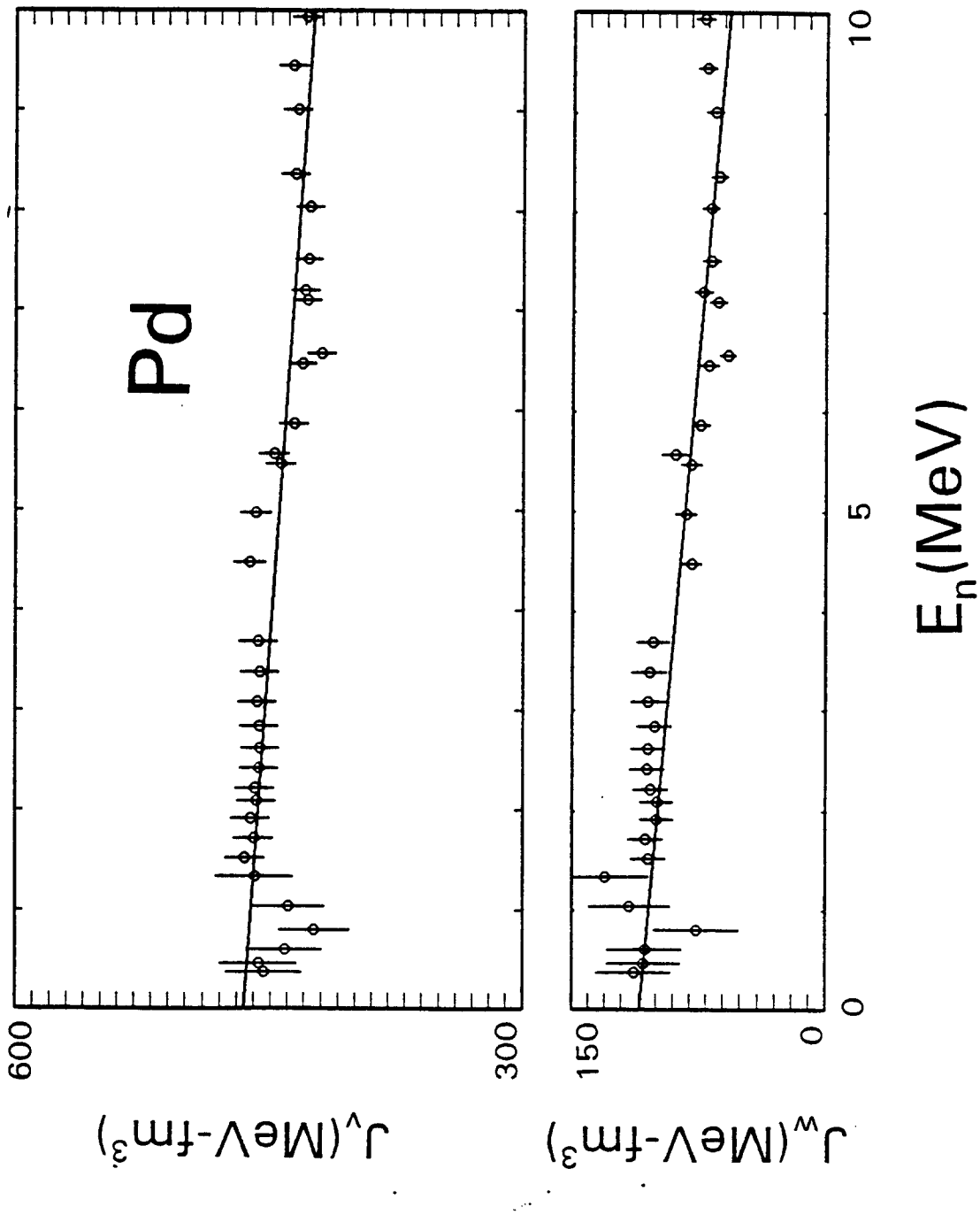

Fig. IV-1. The real (upper) and imaginary (lower) SOM strengths expressed as volume-integrals per nucleon. Curves are taken from Table IV-1 and the symbols refer to individual fits.

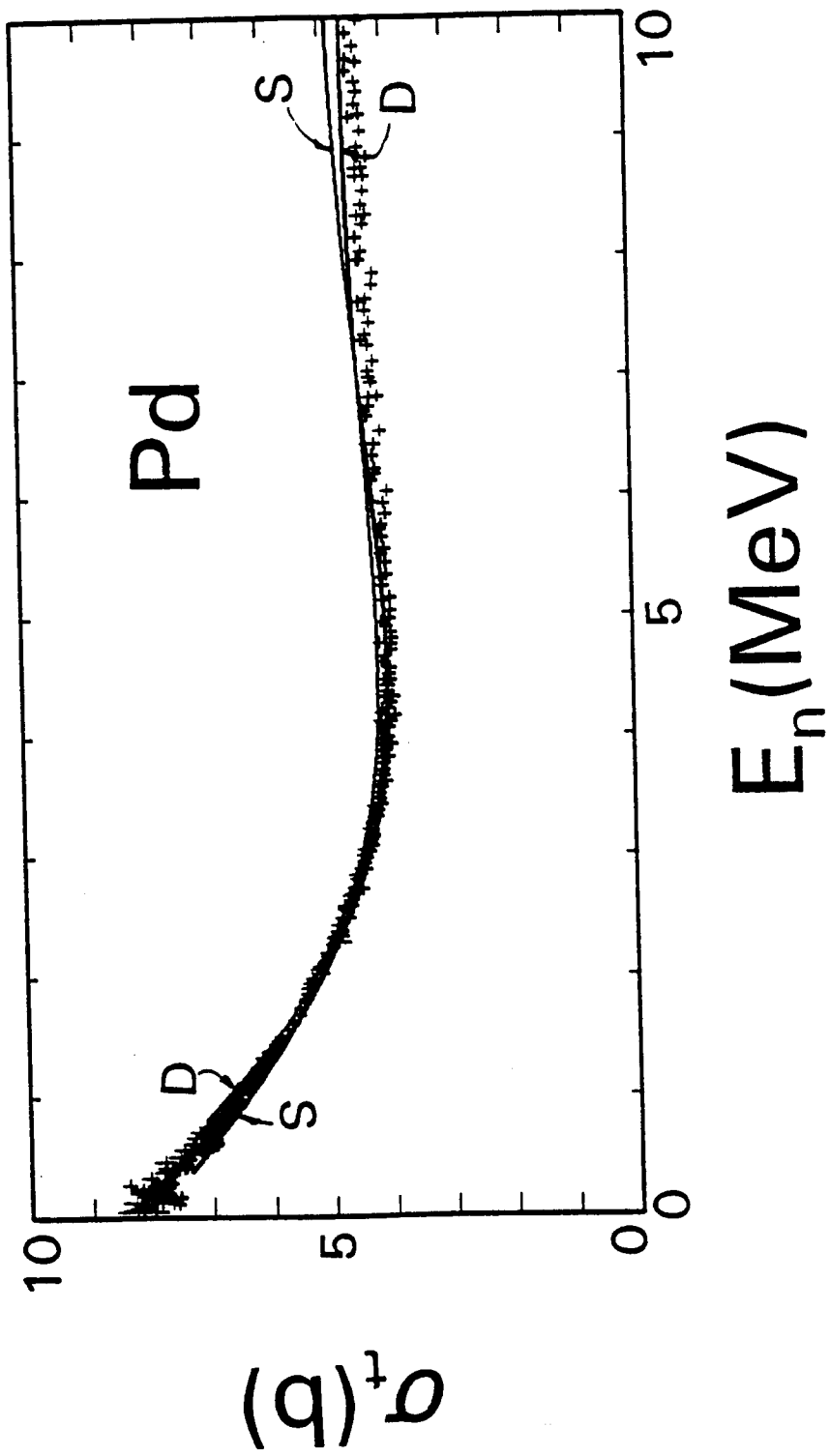

Fig. IV-2. Comparison measured (symbols) and calculated (curves) total cross sections of palladium. Curve "S" indicates the result obtained with the SOM, and "D" that obtained with the CCM, as described in the text.

elastic-scattering always included the first several inelastic-neutron groups from ^{105}Pd. Thus, above 4 MeV the calculations were arranged to fit the composite contributions of elastic and inelastic scattering, and also the better resolved elastic distributions in the 5.5 → 8.0 MeV range, in a way consistent with the measurements. All the fitting procedures were carried out with the computing code ANLECIS [34], following the same six steps outlined above for the SOM derivation.

The resulting CCM parameters are given in Table IV-3, and the energy dependence of the real and imaginary strengths are illustrated in Fig. IV-3. The simple one-phonon model outlined above should be extended to include coupling to the 2^+, 0^+ and 4^+ two-phonon levels at ≈ 1.2 MeV. Comprehensive fitting, such as described above, using an extended one- and two-phonon model is prohibitively time consuming. Therefore, it was assumed that the parameters of Table IV-3 would not be significantly distorted by the introduction of the two-phonon coupling (this was verified by fitting at several isolated energies) and the observables calculated using the parameters of Table IV-3 and the one- and two-phonon model. The two-phonon vibrational states were assumed to be the 1.128 (2^+), 1.134 (0^+) and 1.229 (4^+) levels of ^{106}Pd. The calculated results gave a very good description of the elastic-scattering data base from which the CCM was derived, as shown in Fig. IV-4. At the lower incident energies the first minimum of the distributions may not be accurately reproduced but the discrepancies are small (a few mb) and well within the uncertainties associated with the subtraction of the CN component. The 4.5 → 6.0 MeV region is well represented, in contrast to the SOM results. The calculated total cross sections are in quite close agreement with the measured values, as shown in Fig. IV-3, a better agreement than obtained with the SOM. The DR inelastic-scattering cross sections are shown in Figs. III-6 and IV-5. Combined with CN contributions, the calculated cumulative cross sections for excitations of ≤ 600 keV are in reasonably good agreement with the observed values. The measured results are somewhat lower than the calculations in the ≈ 3 → 4 MeV range but in this region the measured values may be systematically biased as the inelastic component was not well resolved at forward angles where the cross section is large. The experimental situation was further complicated by the presence of the second neutron group from the ^{7}Li source reaction, as noted in Section III. Above ≈ 5 MeV the calculations are slightly larger than the measured values as the entire relevant strength from ^{105}Pd was probably not included in the measurements. The calculated inelastic-scattering angular distributions are qualitatively consistent with the observations as illustrated by the "B" curve in Fig. III-7. The S_0 strength function predicted by the CCM is 0.95 (referenced to A ≡ 106.7), somewhat large than that deduced from resonance measurements [24].

Table IV-3. Palladium CCM parameters determined from the fitting procedures of the text assuming one-phonon excitations and $\beta_2 = 0.235$. The notation is identical to that of Table IV-1.

Real Potential

$$J_V = 422.63 - 2.3722 \cdot E \quad \text{MeV-fm}^3$$
$$r_V = 1.2143 \quad \text{fm}$$
$$a_V = 0.7324 \quad \text{fm}$$

Imaginary Potential

$$J_W = 36.27 + 2.1848 \cdot E \quad \text{MeV-fm}^3$$
$$r_W = 1.4945 - 0.01891 \cdot E \quad \text{fm}$$
$$a_W = 0.3341 + 0.02881 \cdot E \quad \text{fm}$$

Spin-Orbit Potential (Same as given in Table IV-1)

Deformation

$$\beta_2 = 0.235$$

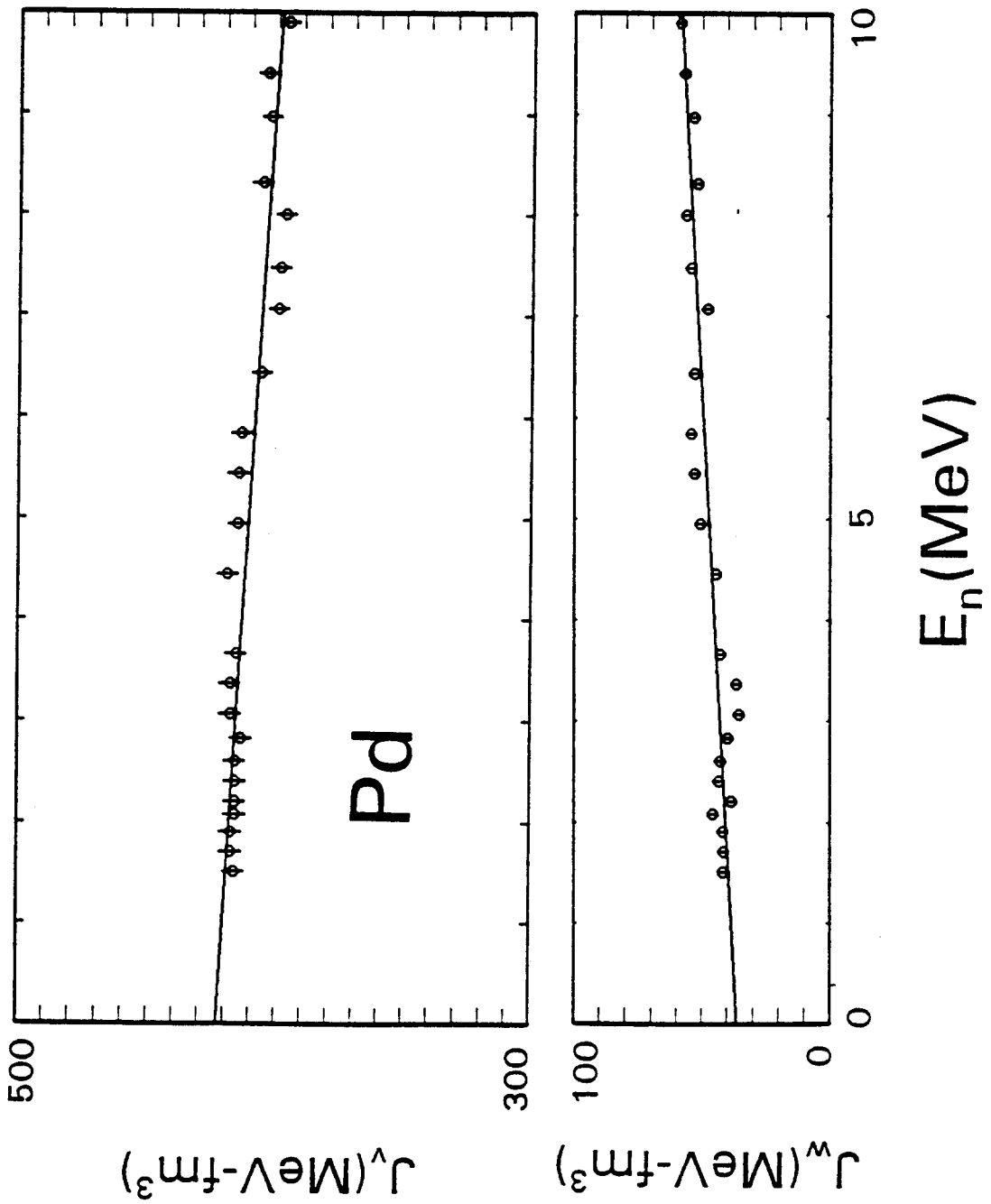

Fig. IV-3. The real (upper) and imaginary (lower) CCM ($\beta_2 \equiv 0.235$) strengths expressed as volume-integrals-per-nucleon as numerically given in Table IV-3.

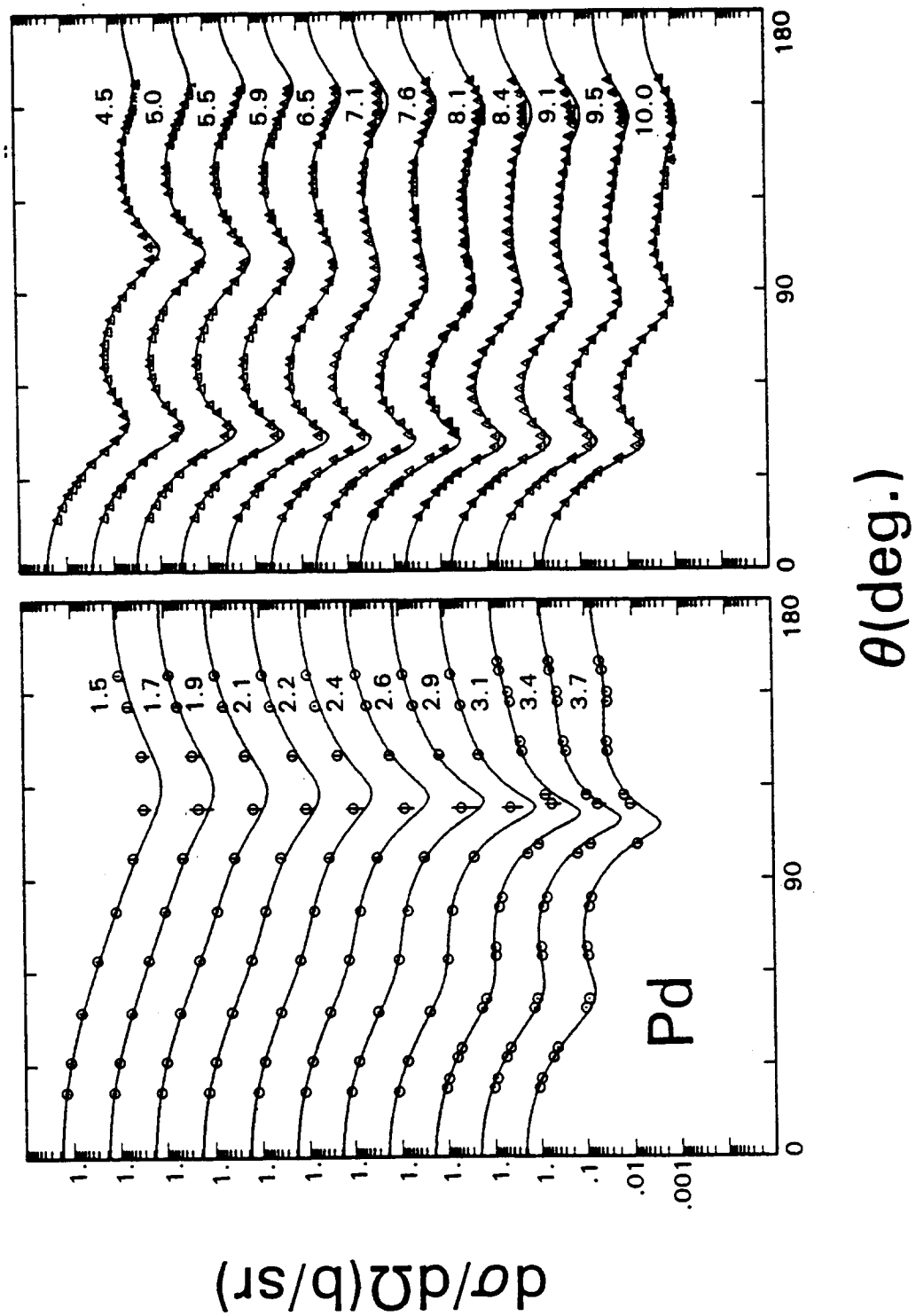

Fig. IV-4. CCM ($\beta_2 \equiv 0.235$) elastic-scattering cross sections (curves) compared with the data base (symbols) from which they were developed. "O" symbols denote elastic scattering, and "Δ" symbols elastic scattering inclusive of contributions from the direct excitation of levels at energies of $\leq$ 600 keV. Numerical values indicate approximate incident-neutron energies. The potential is that of Table IV-3.

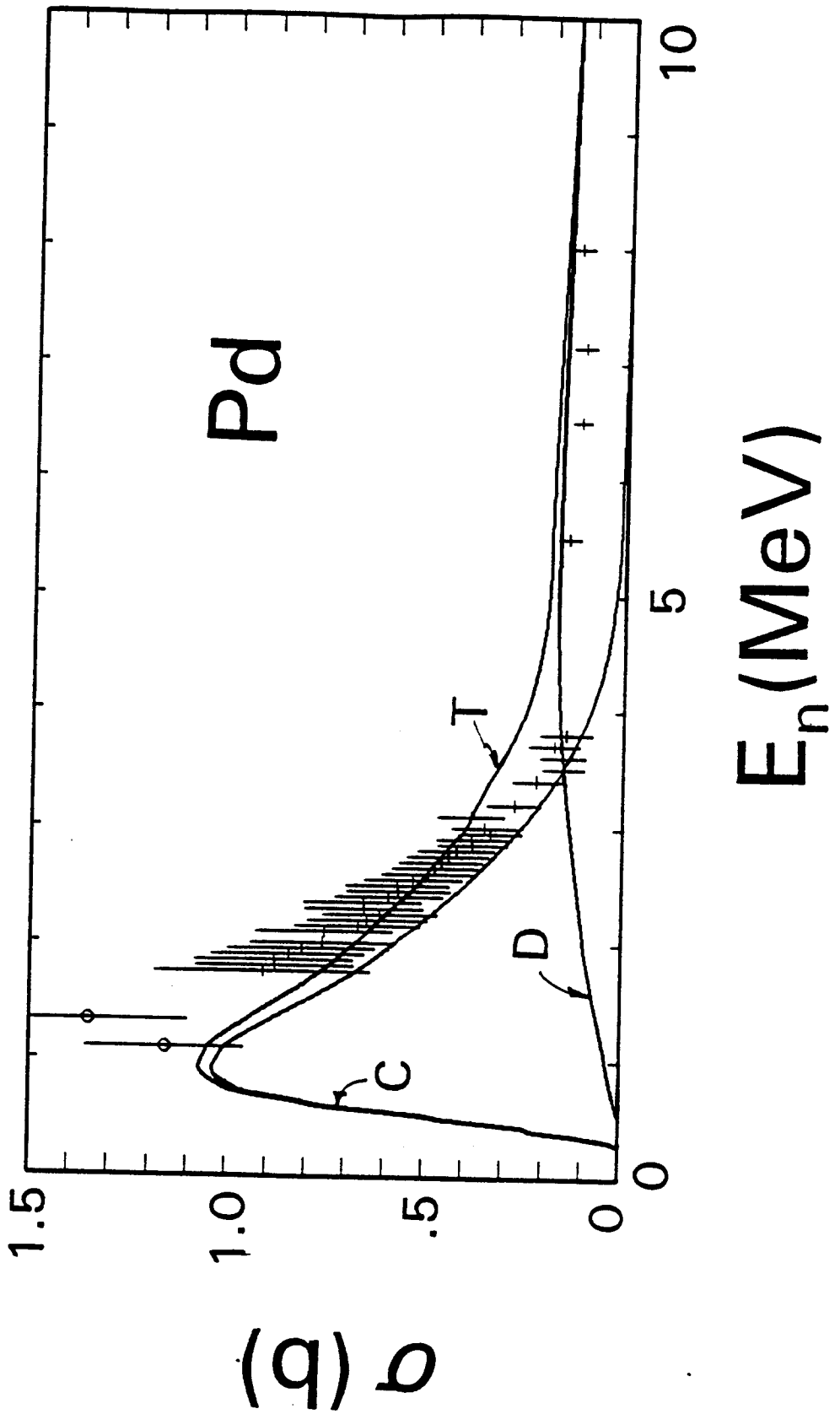

Fig. IV-5. Measured and calculated cumulative excitations of of levels of palladium up to 600 keV. "O" symbols indicate the measured values of ref. [5] and "+" those of the present work. Curves denote; C = CN contribution, D = DR contribution, and T = C + D. The figure is further defined in the text.

If the two-phonon coupling is not included, the calculated results will be ≈ 75% larger than the observed inelastic-scattering cross sections above ≈ 5 MeV. The shortfall can be remedied by considerably reducing β_2. This option was examined by repeating the above extensive CCM fitting procedures using a $\beta_2 = 0.180$, resulting in the model parameters of Table IV-4. The real potential is very similar to that obtained above with $\beta_2 = 0.235$ and essentially equivalent descriptions of the observables were obtained. However, the imaginary potential is quite different, being much larger and decreasing with energy in a manner that is physically unattractive. This behavior is illustrated in Fig. IV-6. Aspects of this alternative CCM are discussed in Section V.

V. DISCUSSION AND SUMMARY

The simple SOM has practical uses but it is inherently inconsistent with some aspects of the fast-neutron interaction with a strong collective vibrator, as in this case. These shortcomings are reflected in the model parameters of Table IV-1. The a_v magnitude is reasonably consistent with "global" trends. However, r_v is relatively large compared to the systematics of SOMs at 8 MeV where $r_v \approx 1.154 + 0.407/A^{1/3}$, or 1.2399 for palladium [35,36]. The palladium J_v is relatively large at low energies, and falls with energy in a rather rapid manner. At 8 MeV SOM systematics predict a $J_v \approx 236.1 \cdot [1 - \xi(N-Z)/A] \cdot (1.154 + 0.407/A^{1/3})^3$, or 415 MeV-fm^3 for palladium [35,36]. This is significantly smaller than the 436 MeV-fm^3 implied by Table IV-1. The r_w is even larger than r_v, and that contributes to the small S_0 values in this mass region, as noted above. The J_w is very large and decreases with energy in a physically difficult to understand manner. The a_w is small at E = 0 and increases with energy. Generally, the present palladium SOM parameters are very much like those recently found for the similar ^{103}Rh nucleus [11]. Possibly the only significant differences are in the details of a_w, and even there they are compensated for by small variations in the J_w's. The unusual behavior of the palladium SOM parameters, particularly the rapid decrease of J_w with energy, reflects the use of that simple model in the context of a strong collective vibrator. This has been generally shown [37], and specifically so in the case of the neighboring ^{103}Rh [11], by the use

Table IV-4. Palladium CCM parameters determined from the fitting procedures of the text assuming one-phonon excitations with $\beta_2 = 0.180$. The notation is identical to that of Table IV-1.

Real Potential

$$J_v = 424.3 - 1.996 \cdot E \quad \text{MeV-fm}^3$$
$$r_v = 1.1993 \quad \text{fm}$$
$$a_v = 0.7283 \quad \text{fm}$$

Imaginary Potential

$$J_w = 63.42 - 1.213 \cdot E \quad \text{MeV-fm}^3$$
$$r_w = 1.473 - 0.0139 \cdot E \quad \text{fm}$$
$$a_w = 0.203 + 0.0517 \cdot E \quad \text{fm}$$

Spin-Orbit Potential (Same as given in Table IV-1)

Deformation

$$\beta_2 = 0.180$$

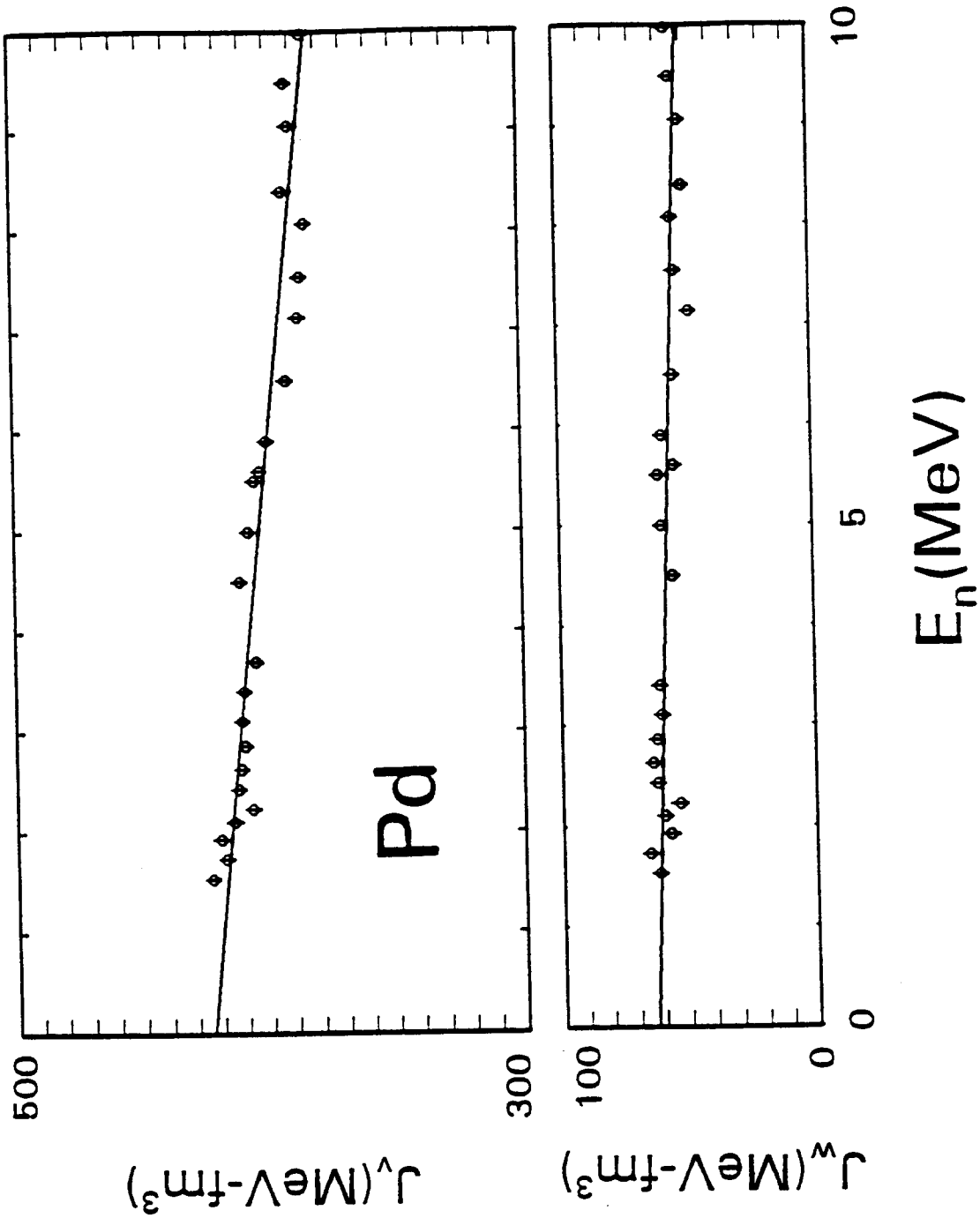

Fig. IV-6. The real(upper) and imaginary (lower) CCM ($\beta_2 \equiv 0.180$) strengths expressed as volume-integrals-per-nucleon.

of numerical simulations.

It is known that the real and imaginary SOM potentials are correlated through the dispersion relationship [38], and that this can lead to energy-dependent geometric parameters and to the correlation of the model in bound and unbound energy regimes. However, these effects are very much obscured in SOM interpretations of the present type, as illustrated by the study of ^{103}Rh described in ref. [11]. The dispersive effects are much smaller than the distortions inherent in the use of a SOM in the context of a strong collective vibrator. Because of this reality, and the complex multi-isotopic nature of elemental palladium, no attempt was made to consider dispersion effects in the present work.

The r_v of the CCM (Table IV-3) is $\approx$ 2% smaller than indicated by systematics [35,36], in contrast to the adjacent ^{103}Rh where it is $\approx$ 1.6% larger [11]. These differences probably are not significant as the real-potential radius is strongly correlated with the real-potential depth and thus difficult to explicitly determine. In fact, the scatter in r_v values during the above CCM fitting procedures was larger than observed on many occasions. The a_v is smaller than that of ^{103}Rh, and nearer the values observed for a number of spherical targets at this laboratory. The J_v is $\approx$ 6% smaller than observed for ^{103}Rh, with approximately the same energy dependence. This difference was not sensitive to the use of one- or one- and two-phonon models. It may be associated with the fact that ^{103}Rh is an odd target that was approximated with a simple even target in the study of ref. [11]. However, J_v is approximately proportional to r_v^3 therefore sensitive to r_v, and that of palladium and of ^{103}Rh [11] are somewhat different. An alternative measure of potential strength is the second moment, $V \cdot r_v^2$ [31], which is rigorously valid for a square well. $V \cdot r_v^2$ of palladium and ^{103}Rh differ by only 1.4%. Numerical simulations suggest that, in some cases, $V \cdot r_v^2$ is a better parameter than J_v for comparing potential strengths [39]. The use of various moments in the parameterization of real-potential strengths is extensively discussed by Mahaux and Sartor [40]. The present CCM palladium J_v is quite similar to that proposed for global spherical models; for example, the difference between the results of ref. [41] and that of the present work is $\approx$ 0.8% at 8 MeV. However, the energy dependence of the J_v of the global models is considerably greater than that of the present work. This is likely an example of the reduced

energy dependence of the strength, within several-tens of MeV of the Fermi Surface, from the general long-range trends of the equivalent-local Hartree-Fock potential [41]. The dynamic vibrational model of Brown et al. [42] suggests that $dV/dE|_{E\to 0} \approx -0.19$ for palladium, compared to the present CCM value of ≈ -0.27. An interpretation based upon a wider energy scope might well show a slope of the strength nearer that of the suggested global models.

The influence of the CCM is most evident in the imaginary potential. Using the EM β_2 value [33], a rather small J_w, that increases with energy in a physically reasonable way, is obtained. In the framework of the one-phonon model, the associated inelastic excitations of the one-phonon yrast level is much larger than observed, as indicated by curve "A" of Fig. III-7. When the coupling is extended to include two-phonon levels this drawback is very much alleviated as indicated by curve "B" of Fig. III-7 and curve "D" of Fig. III-6. The alternative of a one-phonon model with a much reduced β_2 value will achieve the same end but will lead to much larger J_w strengths at lower energies that decrease with energy in a way that is difficult to physically understand (Table IV-4 and Fig. IV-6). The behavior approaches that observed with the SOM and is a reflection of the use of inappropriate (or non existent) coupling in an interpretation of the neutron interaction with a strong vibrator. The behavior has been numerically demonstrated using simulations [37]. Both one-phonon and one- and two-phonon CCM models give approximately the same relative angular distributions, as illustrated in Fig. III-7, and they both qualitatively follow the measured shape. The one- and two-phonon model continues to somewhat over-predict the inelastic cross section. This is probably partly due to the failure of the measurements to include all relevant contributions from ^{105}Pd. In addition, there are doubtless other minor couplings, beyond those of the one- and two-phonon model, involved and their introduction will reduce the calculated cross section for the excitation of the yrast 2^+ level. If these latter effects amount to an $\approx$ 25% reduction in the calculated result, one obtains the "C" curve of Fig. III-7 which is in reasonable agreement with the differential values (and with the angle integrated values of Fig. IV-5). An analogous effect has been observed in neutron scattering from the cadmium isotopes [10]. The present CCM does not deal with individual isotopes. Of course, these too will be subject to DR effects, and they will increase the calculated cross sections for the excitation of 306 and 411 keV levels from the CN component shown in Fig. III-6 and result in an improved agreement with experiment.

In comparing neutron and EM deformations, one should use deformation lengths, $\delta_i \equiv r_i \cdot \beta_2$. EM considerations are based upon a r_v = 1.2 fm [33]. This implies a δ_{em} = 0.282, to be compared with the δ_n = 0.285 employed in the present one- and two-phonon CCM. The

difference is not significant, but it has been theoretically suggested that δ_{em} is slightly less than δ_n [43]. It will take far better data than now available to define such small differences. Alternatively, the one-phonon CCM leads to δ_n that is much smaller than δ_{em}, in contrast to theoretical prediction. The r_w of the present CCM is large and very similar to those observed in the cases of other vibrational targets [10,11]. The a_w increases with energy from relatively small values at E = 0, also as commonly encountered [10,11].

While the present measurements encompass the very large majority of all the experimental information relevant to fast-neutron scattering from palladium, they do not extend above 10 MeV, and there is no higher-energy experimental information available elsewhere. Thus the model interpretations are explicitly applicable only up to ≈ 10 MeV. Clearly, some of the energy dependencies of the model parameters can not extend indefinitely, and there must be some approach to asymptotic higher-energy behavior that can not be defined from the available experimental information. In addition, the energy range of the study does not extend far enough to give any realistic assessment of the onset of volume absorption. However, the present work does encompass the large majority of the energy range of applied interest, and the results should prove a suitable vehicle for improving basic data for applications.

Finally, the experimental data reported here has been transmitted to the National Nuclear Data Center, Brookhaven National Laboratory. Those interested in numerical values should contact that Center.

REFERENCES

1. P. De Gelder, E. Jacobs and D. De Frenne, Nucl. Data Sheets 38 545 (1983); R. L. Haese, F. E. Bertrand, B. Harmatz and M. J. Martin, Nucl. Data Sheets 37 289 (1982); B. Harmatz, Nucl. Data Sheets 30 305 (1980); D. De Frenne, E. Jacobs, M. Verboven and P. De Gelder 47 261 (1986); J. Blachot, J. P. Husson, J. Oms and G. Betrier, Nucl. Data Sheets 41 325 (1984); and P. De Gelder, D. De Frenne and E. Jacobs, Nucl. Data Sheets 35 443 (1982).

2. A. B. Smith, P. T. Guenther and J. F. Whalen, Argonne National Laboratory Report, ANL/NDM-71 (1982).

3. H. Gruppelaar and H. A. J. Van der Kamp, NEA Report, NEANDC-222(U) (1985); see also Proc. of Specialist's Meeting on Fission-Product Nuclear Data, NEA report, NSC/DOC(92)9 (1992).

4. D. Cline et al., Measurement of Quadrupole Collective Degrees of Freedom in ^{110}Pd by Coulomb Excitation, private communication, to be published.

5. A. Smith, P. Lambropoulos, P. Guenther and J. Whalen, Nucl. Sci. and Eng. 49 389 (1972).

6. A. Smith, P. Guenther and J. Whalen, Nucl. Phys. A415 1 (1984).

7. S. Chiba, P. Guenther and A. Smith, Ann. Nucl. Energy 16 637 (1989).

8. A. Smith, P. Guenther, J. Whalen and S. Chiba, J. Phys. G18 629 (1992).

9. S. Chiba, P. Guenther, A. Smith, M. Sugimoto and R. Lawson, Phys. Rev. C45 1260 (1992).

10. A. B. Smith and P. T. Guenther, Argonne National Laboratory Report, ANL/NDM-127 (1992).

11. A. B. Smith and P. T. Guenther, Argonne National Laboratory Report, ANL/NDM-130 (1993).

12. W. P. Poenitz and J. F. Whalen, Argonne National Laboratory Report, ANL/NDM-80 (1983).

13. L. Cranberg and J. Levin, Proc. Inter. Conf. on Peaceful Uses of Atomic Energy (United Nations Press, New York, 1955).

14. A. Smith, P. Guenther, R. Larsen, C. Nelson, P. Walker and J. Whalen, Nucl. Instr. Methods 50 277 (1967).

15. M. Drosg, IAEA Report, IAEA-TECDOC-410 (IAEA Press, Vienna, 1987).

16. A. Smith, P. Guenther and R. Sjoblum, Nucl. Instr. Methods 140 397 (1977).

17. A. Smith, P. Guenther and R. McKnight, Proc. Conf. on Nucl. Data for Sci. and Technology, p.-39, Editor K. H. Boeckhoff (Reidel Press, Dordrecht, Holland, 1982).

18. Nuclear Standards File IAEA Tech. Report 227, Editors H. Conde, A. Smith and A. Lorenz (1982).

19. P. T. Guenther, Data acquisition and processing code NEWAGE, Argonne National Laboratory internal memorandum (1992) unpublished.

20. A. B. Smith, Monte-Carlo correction codes MONTESPHERE and MONTEPOLY, Argonne National Laboratory internal memorandum (1991) unpublished.

21. D. Foster and D. Glasgow, Phys. Rev. C3 576 (1971).

22. National Nuclear Data Center, Brookhaven National Laboratory, Upton, New York.

23. A. B. Smith, J. W. Meadows and R. J. Howerton, Evaluated neutronic files for the natural isotopes of palladium, to be published.

24. S. F. Mughabghab, M. Divadeenam and N. E. Holden, Neutron cross sections (Academic, New York, 1981).

25. A. Gilbert and A. Cameron, Can. J. Phys. 43 1446 (1965).

26. W. Hauser and H. Feshbach, Phys. Rev. 87 362 (1952).

27. P. A. Moldauer, Nucl. Phys. A344 185 (1980).

28. P. A. Moldauer, The spherical optical-statistical code ABAREX, private communication (1982).

29. F. D. Becchetti Jr. and G. W. Greenlees, Phys. Rev. 182 1190 (1969).

30. R. L. Walter and P. P. Guss, Proc. Conf. on Nucl. Data for Basic and Applied Science, Editors P. Young et al. (Gordon and Breach, New York, 1986) vol. 2, p. 1079.

31. P. E. Hodgson, Nuclear reactions and nuclear structure (Clarendon, Oxford, 1971).

32. P. A. Moldauer, Nucl. Phys. 47 63 (1963).

33. S. Raman, C. H. Malarkey, W. T. Miller, C. W. Nestor Jr. and P. H. Stelson, Atom. Data and Nucl. Data Tables 36 1 (1987).

34. P. A. Moldauer, The coupled-channels computer code ANLECIS, private communication (1982); a modification of the ECIS code of J. Raynal, NEA memorandum (1979).

35. S. Chiba, P. T. Guenther, R. D. Lawson and A. B. Smith, Phys. Rev. C42 2487 (1990).

36. A. B. Smith and P. T. Guenther, J. Phys. G19 655 (1993).

37. A. B. Smith, Argonne National Laboratory internal memorandum (1990), unpublished.

38. G. R. Satchler Direct nuclear reactions (Clarendon, Oxford, 1983).

39. A. B. Smith, Argonne National Laboratory internal memorandum (1991), unpublished.

40. C. Mahaux and R. Sartor, Nucl. Phys. A458 25 (1986).

41. M. Bauer, E. Hernandez-Saldana, P. E. Hodgson and J. Quintanilla, J. Phys. G8 525 (1982).

42. G. E. Brown, J. S. DeHesa and J. Speth, Nucl. Phys. A330 290 (1979).

43. V. A. Madsen, V. R. Brown and J. D. Anderson, Phys. Rev. C12 1205 (1975).